Trends in Physical Chemistry
Vol. 21, 2021

Review

Gas-phase kinetics of OH-reactions with H_2CO, CH_3OH, and CH_3CH_2OH at very low temperatures: Astrophysical implications

A. J. Ocaña[1,#], B. Ballesteros[1,2], J. Albaladejo[1,2] and E. Jiménez[1,2,*]

[1]Departamento de Química Física, Facultad de Ciencias y Tecnologías Químicas, Universidad de Castilla-La Mancha, Avda. Camilo José Cela, 1B, 13071, Ciudad Real;
[2]Instituto de Investigación en Combustión y Contaminación Atmosférica, Universidad de Castilla-La Mancha, Camino de Moledores s/n., 13071, Ciudad Real, Spain.

ABSTRACT

Up to now, more than 200 molecular species have been detected by the astronomers using ground-based and space-based telescopes within the cold (T<100 K) regions of the so-called interstellar medium (ISM). The hydroxyl (OH) radical is ubiquitous in most of these observations, as well as other molecules such as formaldehyde (H_2CO), methanol (CH_3OH), and ethanol (CH_3CH_2OH). The chemistry in such regions of the ISM requires the knowledge of reliable rate coefficients from laboratory data to interpret the astronomical observations in terms of abundances relative to H nuclei, the most abundant species in the ISM. In this review, the current results on the gas-phase kinetics of reactions of the OH radical with H_2CO, CH_3OH and CH_3CH_2OH at T<202 K are presented. In these studies, to generate a uniform well-controlled cold environment and performing the kinetic experiments, the CRESU (French acronym of *Cinétique de Réaction en Ecoulement Supersonique Uniforme*) technique is mostly employed. This technique is based on a continuous or pulsed supersonic expansion of a gas from a high-pressure *reservoir* to a low-pressure chamber through a "tunable" Laval nozzle coupled to different detection methods such as laser-based techniques. The pulsed CRESU technique has been used by the UCLM research group to study chemical kinetics at ultralow temperatures (T = 11.7 - 177.5 K). This apparatus achieves the lowest temperature ever reached with a pulsed CRESU, 11.7 K. The reviewed results have important implications in the interdisciplinary field of Astrochemistry as an enhancement of the rate coefficient for the title reactions has been observed, providing more realistic data than those derived from extrapolation of temperature dependencies obtained at high temperatures usually employed in astrochemical models in the absence of low temperature data. In addition, these kinetic results help to shed some light on the astronomical observations of HCO and CH_3O radicals in dark molecular clouds of the ISM.

KEYWORDS: interstellar chemistry, kinetics, gas-phase, CRESU technique, modelled abundances.

INTRODUCTION

The modern Astronomy has unveiled that the hydroxyl (OH) radical is ubiquitous within the cold regions of the interstellar medium (ISM) as dark molecular clouds or star-forming regions (T<100 K) where formaldehyde (H_2CO), methanol, (CH_3OH) and ethanol (CH_3CH_2OH) are also

*Corresponding author: Elena.Jimenez@uclm.es

[#]Currently at Sorbonne Université, Observatoire de Paris, Université PSL, CNRS, LERMA, F-75005 Paris, France.

identified − see McGuire *et al*. and references therein [1]. These molecules are thought to be mainly formed under the extreme temperature (*T*~8−15 K) inherent to the dark interstellar clouds [2]. Predominantly, in the condensed phase, these oxygenated molecules may be formed by successive hydrogenation steps in CO-rich icy mantles of interstellar dust grains to finally be released to the gas phase where they are detected after the warm-up phase or by non-thermal desorption processes [3, 4]. Nevertheless, their formation on grain surfaces cannot fully explain the observed abundances of these species in the ISM with respect to the H nuclei − by far the most abundant species [5]. In order to explain the abundances of IS species, complex and multivariant astrochemical models are developed by astronomers and astrophysicists. These models need, among other parameters, reliable rate coefficients (*k*) for all the reactions involved at very low temperatures typical of the ISM. Paradoxically, and due to the lack of experimental data, the astrochemical models usually use *k* values extrapolated from temperature dependencies reported at *T* >200 K as well as an arbitrary value of 10^{-11} cm^3 s^{-1}, even though it is known that the rate coefficient for many chemical reactions is enhanced at very low temperatures [6]. In the last few decades, many astrophysics and astrochemistry laboratories have dedicated to study experimentally the kinetics of OH-reactions with H_2CO, CH_3OH and CH_3CH_2OH at very low temperatures using the well-known CRESU technique with the final goal of providing to the scientific community consistent rate coefficients to be included in astrochemical models [7-13].

From a chemical point of view, what is common in the reviewed reactions is that they take place *via* the exothermic H-abstraction by the OH radical with the consequent formation of H_2O [14]. The reactivity of OH radicals with oxygenated organic molecules has been observed to be accelerated at very low temperatures. These observations have been theoretically interpreted by the formation of a long-lived pre-reaction complex, which evolves to the products facilitated by quantum mechanical tunnelling (QMT) despite the reaction barrier. The lifetime of the so-called pre-reaction complex depends not only on the temperature, but also on the density of the vibrational states; for large molecules such as CH_3OCH_3, this complex has a lifetime of ~10^{-3} s at 93 K while for smaller molecules such as CH_3OH, it is about ~2.7 μs at 93 K [6].

For the H_2CO + OH reaction, the formation of formyl (HCO) radicals in the gas-phase according to R1 has been previously invoked to explain the astronomical observations of this radical in interstellar envelopes [15].

$$H_2CO + OH \rightarrow HCO + H_2O \qquad \Delta H_{298} = -127 \text{ kJ mol}^{-1} \qquad \text{(R1)}$$

The gas-phase CH_3OH + OH reaction (R2), is the one in which the astrochemical community have been focused with more effort in the last years due to the relatively high abundance of methanol in different astrochemical environments, $10^{-6} - 10^{-7}$ in hot cores, 10^{-9} in dark molecular clouds, and $<10^{-9}$ in diffuse clouds [16]. Reaction R2 can proceed *via* two different pathways, the H-atom abstraction from the OH group (R2.1) or the methyl group (R2.2).

$$CH_3OH + OH \rightarrow CH_3O + H_2O \qquad \Delta H_{298} = -60.2 \text{ kJ mol}^{-1} \qquad \text{(R2.1)}$$

$$\rightarrow CH_2OH + H_2O \qquad \Delta H_{298} = -95.2 \text{ kJ mol}^{-1} \qquad \text{(R2.2)}$$

The methoxy (CH_3O) radical has been detected in the ISM, concretely in the dark molecular cloud Barnard 1b [17]; however despite the efforts of the astronomers, the hydroxymethyl (CH_2OH) radical has not been identified yet. Cernicharo *et al.* [17] suggested that reaction (R2.1) could be a potential source of CH_3O in Barnard 1b.

The third chemical reaction presented in this review, the CH_3CH_2OH + OH reaction (R3) has recently gained interest in the astrochemical community as it can be a hypothetical starting point for the production of other complex organic molecules (COMs), *e.g.* glycolaldehyde, acetic acid and formic acid [18]. The hydrogen atom abstraction reaction, in CH_3CH_2OH, can proceed *via* three different pathways as follows:

$$CH_3CH_2OH + OH \rightarrow CH_3CH_2O + H_2O \qquad \Delta H_{298} = -59.7 \text{ kJ mol}^{-1} \qquad \text{(R3.1)}$$

$$\rightarrow CH_3CHOH + H_2O \qquad \Delta H_{298} = -95.8 \text{ kJ mol}^{-1} \qquad \text{(R3.2)}$$

$$\rightarrow CH_2CH_2OH + H_2O$$
$$\Delta H_{298} = -67 \text{ kJ mol}^{-1} \quad \text{(R3.3)}$$

Despite its potential as a precursor of COMs neither of the radical products of R3.1, R3.2 and R3.3 have been detected yet in the interstellar medium.

The knowledge of the branching ratios (BRs) for reactions R2 and R3 is a key issue in astrochemical modelling since the chemistry of the ISM may change depending on the reaction products. BRs can be experimentally determined by different methods, like mass spectrometry, and laser induced fluorescence (LIF) or by investigating the kinetics of deuterated analogues [19]. Particularly, for reaction (R3), the product branching ratios are unknown at very low temperatures. Regarding reaction (R2), Shannon *et al*. [11] experimentally confirmed the formation of CH_3O radical in reaction (R2.1) by using LIF in CRESU experiments at T = 82 K [11] and tried the detection of the CH_3CH_2O radical (R3.1), but failed [13]. In addition to laboratory methods, computational studies can also be carried out to determine the BRs. Several studies concerning the branching ratios can be found in the bibliography, and these studies are briefly presented in the discussion section of this review [20]. The implications of reactions (R1) and (R2) on the interpretation of observed abundances of HCO and CH_3O radicals in dark molecular clouds will be discussed as well.

METHODS

The experimental results presented here were obtained by using mainly a CRESU apparatus. In case of the results provided by the research group of the University of Castilla-La Mancha (UCLM), the experimental setup is described in detail in Ref. [21], while for the data reported by the University of Leeds, the description of the apparatus can be found in Ref. [22]. In addition, the Leeds research group has combined their CRESU results with other results obtained by using a flow tube to reach very low temperatures [12, 13]. The CRESU technique is based on the uniform supersonic expansion of a gas from a high-pressure reservoir (P_{res}) to a low-pressure chamber (P_{cham}) through a Laval Nozzle. The technique was recently adapted by the research group FOTOAIR of the UCLM to go beyond the state-of-the-art by using a rotatory disk (chopper) developed in collaboration with researchers of the University of Rennes 1 (France). The improvements related to the development of the pulsed mode overcome the difficulties intrinsic to the technique, *i.e.* high gas consumption and pumping capacities [21]. In addition, a new methodology based on the mixing of rare gases was implemented to fine-tune the supersonic jet temperature with a reduced number of Laval nozzles [23]. Pushing the limits of our experimental setup, a new nozzle was designed to obtain the lowest temperature ever achieved using the pulsed CRESU, 11.7 K [9]. There are other alternatives to pulse the gas flow such as the employment of a pulsed valve; this is the method used by the research group of the University of Leeds [22]. Concerning the fundamentals of the technique, only a brief description is given as follows. The properties of the supersonic jet, formed mainly by a buffer inert gas (He, N_2, Ar or binary mixtures He/N_2 or Ar/N_2), are defined by the Mach number (M). This parameter is calculated from impact pressure measurements using a fast Pitot tube [21, 23]. The mean temperature (T) and density (n) of the supersonic jet relative to the temperature and molecular density in the *reservoir*, T_0 and n_0, respectively, can be computed using the following expressions:

$$\frac{T_0}{T} = 1 + \frac{\gamma-1}{2} M^2 \quad \text{Eq. 1}$$

$$\frac{n_0}{n} = \left(\frac{T_0}{T}\right)^{\frac{1}{\gamma-1}} \quad \text{Eq. 2}$$

where γ is the ratio of specific heats of the buffer gas. Notice that to reach lower temperatures and densities higher supersonic jet speed is required *i.e.*, higher M values as demonstrated mathematically according to Equations 1 and 2. In Table 1, a summary of the operational conditions available at the University of Castilla-La Mancha at temperatures up to 177.5 K is given, *i.e.* temperature, gas density, Mach number, buffer gases, pressure in the reservoir and pressure in the chamber. The data at similar temperature are listed in terms of increasing atomic/molecular density.

Table 1. Supersonic flow physical properties and pressure conditions required for generating the jet between 11.7 and 117.5 K.

T_{typ}/K	T/K	$n/10^{16}$ cm^{-3}	M	Bath gas	P_{res}/mbar	P_{cham}/ mbar
	11.7 ± 0.7	6.88 ± 0.62	8.56 ± 0.26	He	366.48	0.117
	13.0 ± 0.7	6.41 ± 0.55	8.04 ± 0.24	He	280.16	0.117
	14.3 ± 0.8	5.90 ± 0.52	7.75 ± 0.24	He	236.75	0.122
~21	22.1 ± 1.4	1.91 ± 0.25	7.05 ± 0.24	N_2/He	140.81	0.071
	21.1 ± 0.6	3.37 ± 0.15	6.27 ± 0.10	He	73.88	0.125
	22.5 ± 0.7	7.43 ± 0.32	6.05 ± 0.09	He	147.76	0.280
	21.7 ± 1.4	16.65 ± 1.61	6.13 ± 0.21	He	337.20	0.620
	36.2 ± 1.2	17.73 ± 0.86	4.65 ± 0.08	He	173.32	1.100
	42.6 ± 1.3	5.22 ± 0.33	5.02 ± 0.08	N_2/He*	127.05	0.296
~45	45.5 ± 2.0	0.69 ± 0.08	5.26 ± 0.13	N_2	31.17	0.050
	45.3 ± 1.3	4.23 ± 0.28	5.06 ± 0.08	N_2/He	132.23	0.295
	45.6 ± 1.4	10.19 ± 0.52	4.34 ± 0.08	N_2/He	102.96	0.740
~50	50.5 ± 1.6	1.50 ± 0.12	4.94 ± 0.10	N_2	52.12	0.120
	51.6 ± 1.7	4.17 ± 0.35	4.88 ± 0.10	N_2*	136.24	0.279
	49.9 ± 1.4	8.33 ± 0.41	4.23 ± 0.07	N_2/He	86.00	0.650
	52.1 ± 0.5	19.52 ± 0.28	3.76 ± 0.02	Ar	110.15	1.500
	55.4 ± 1.4	3.02 ± 0.23	4.66 ± 0.08	N_2	81.49	0.216
~64	64.1 ± 1.7	2.24 ± 0.15	4.25 ± 0.07	N_2*	41.70	0.180
	64.1 ± 1.6	4.63 ± 0.27	4.09 ± 0.07	N_2/He	65.47	0.45
	64.4 ± 0.6	17.36 ± 0.29	3.60 ± 0.02	N_2/Ar	112.60	1.670
~70	69.5 ± 1.6	3.26 ± 0.19	4.04 ± 0.06	N_2	50.57	0.360
	68.8 ± 0.6	16.58 ± 0.27	3.55 ± 0.02	N_2/Ar	110.53	1.690
~80	78.2 ± 1.0	2.45 ± 0.08	3.74 ± 0.03	N_2*	28.56	0.283
	81.1 ± 0.5	14.49 ± 0.22	3.44 ± 0.02	N_2/Ar	105.66	1.720
~90	92.5 ± 0.5	13.09 ± 0.19	3.33 ± 0.01	N_2	101.15	1.770
	89.5 ± 0.6	18.24 ± 0.33	3.40 ± 0.02	N_2	151.59	2.370
	89.1 ± 0.7	43.38 ± 0.51	2.65 ± 0.01	Ar	109.73	5.960
~100	99.3 ± 0.4	7.67 ± 0.09	3.16 ± 0.01	N_2	49.51	1.140
	101.8 ± 0.6	18.34 ± 0.17	2.39 ± 0.01	Ar	37.66	3.053
~107	107.0 ± 0.5	4.90 ± 0.06	2.98 ± 0.01	N_2	26.12	0.790
	106.0 ± 0.6	14.02 ± 0.11	2.32 ± 0.01	Ar	27.09	2.515
	115.3 ± 1.1	9.58 ± 0.14	2.16 ± 0.02	Ar	16.16	1.964
	122.5 ± 1.0	7.20 ± 0.08	2.07 ± 0.01	Ar	11.28	1.600

Table 1 continued..

T_{typ}/K	T/K	$n/10^{16}$ cm^{-3}	M	Bath gas	P_{res}/mbar	P_{cham}/ mbar
	136.1 ± 0.8	24.92 ± 0.35	2.43 ± 0.01	N_2	71.99	5.200
~141	140.4 ± 1.0	21.68 ± 0.40	2.36 ± 0.01	N_2	57.94	4.707
	143.3 ± 0.6	17.02 ± 0.17	2.32 ± 0.01	N_2	43.77	3.822
~150	148.3 ± 0.6	12.35 ± 0.13	2.24 ± 0.01	N_2	29.10	2.923
	149.9 ± 0.7	10.69 ± 0.12	2.21 ± 0.01	N_2	24.25	2.607
	153.1 ± 0.7	9.14 ± 0.11	2.15 ± 0.01	N_2	19.42	2.281
	158.8 ± 0.6	7.40 ± 0.07	2.07 ± 0.01	N_2	14.37	1.961
	165.7 ± 0.9	5.64 ± 0.08	1.98 ± 0.01	N_2	9.96	1.566
	177.5 ± 1.2	6.71 ± 0.11	1.83 ± 0.02	N_2	9.97	2.000

*****Continuous mode. Uncertainties are ±σ (standard deviation) for T and n.

Using the supersonic jet as the reactive medium and after the synchronization with laser techniques to probe the chemistry, reliable rate coefficients are determined by several measurements of the time-resolved fluorescence signal at λ~310 nm emitted from the OH($A^2\Sigma^+$) in electronic excited state, previously reached by exciting OH($X^2\Pi$). The so-called laser induced fluorescence ($I_{LIF,t}$) is detected by a photomultiplier tube (Electron Tube, model 9813B) and its temporal profile is recorded both in the absence and in the presence of different concentrations of R (H_2CO, CH_3OH or CH_3CH_2OH) as explained by Ocaña *et al*. [7-9].

Figure 1 shows two examples of the OH radical fluorescence over the reaction time in the presence of CH_3OH and CH_3CH_2OH collected after the signal processing using a boxcar integration unit (Stanford Research Systems, model SR250) connected to the photomultiplier tube. Notice that the data points can be fitted to a biexponential adjustment considering the temporal evolution of the OH radical according to equation 3, the residual data being the deviation of the experimental data from the fit.

$$[OH]_t = \left(\frac{k'_{rel}}{k'-k'_{rel}}\right)[OH^*]_0\left(e^{-k'_{rel}\,t} - e^{-k't}\right) + [OH]_0 e^{-k't} \qquad \text{Eq. 3}$$

where k'_{rel} and k' are the *pseudo*-first order rate coefficients for the rotational relaxation of excited OH* and for the OH-reaction with R. The subscripts 0 and t correspond to the OH (or OH*) concentrations at a time t and t = 0, respectively. As we measure the laser-induced fluorescence emitted by the OH radical, equation 3 can be rewritten as:

$$I_{LIF,\,t} = A\left(e^{-k'_{rel}\,t} - e^{-k't}\right) + Be^{-k't} \qquad \text{Eq. 4}$$

where A is a factor linked with the contribution of OH* rotational relaxation to the measured, $I_{LIF,t}$ and B is a factor associated with the initial OH concentration at t = 0, just after the photolysis pulse.

After the OH production, the observed increase in the $I_{LIF,t}$ is the result of an increase in the ground state OH. The rotational relaxation process occurs, depending on temperature and the concentration of collisional partner, at a few tens of microseconds (t_0 ~ 25-50 μs). Figure 1 shows the exponential decay observed after OH* is relaxed, which is due to the depletion of OH by reaction with R. From the analysis of such decays, the k' values can be derived from equations 5 or 6.

$$I_{LIF,\,t} = I_{LIF,\,0}\exp\{-k'\,(t\text{-}t_0)\} \qquad \text{Eq. 5}$$

$$ln\, I_{LIF,\,t} = ln\, I_{LIF,\,0} - k'(t\text{-}t_0) \qquad \text{Eq. 6}$$

In Figure 2, several data computed from Eq. 6 at a fixed temperature and varying [CH_3OH] are shown. The values of k' obtained from the slope of these linear plots are included in the figure. Only three single experiments are represented in Figure 2

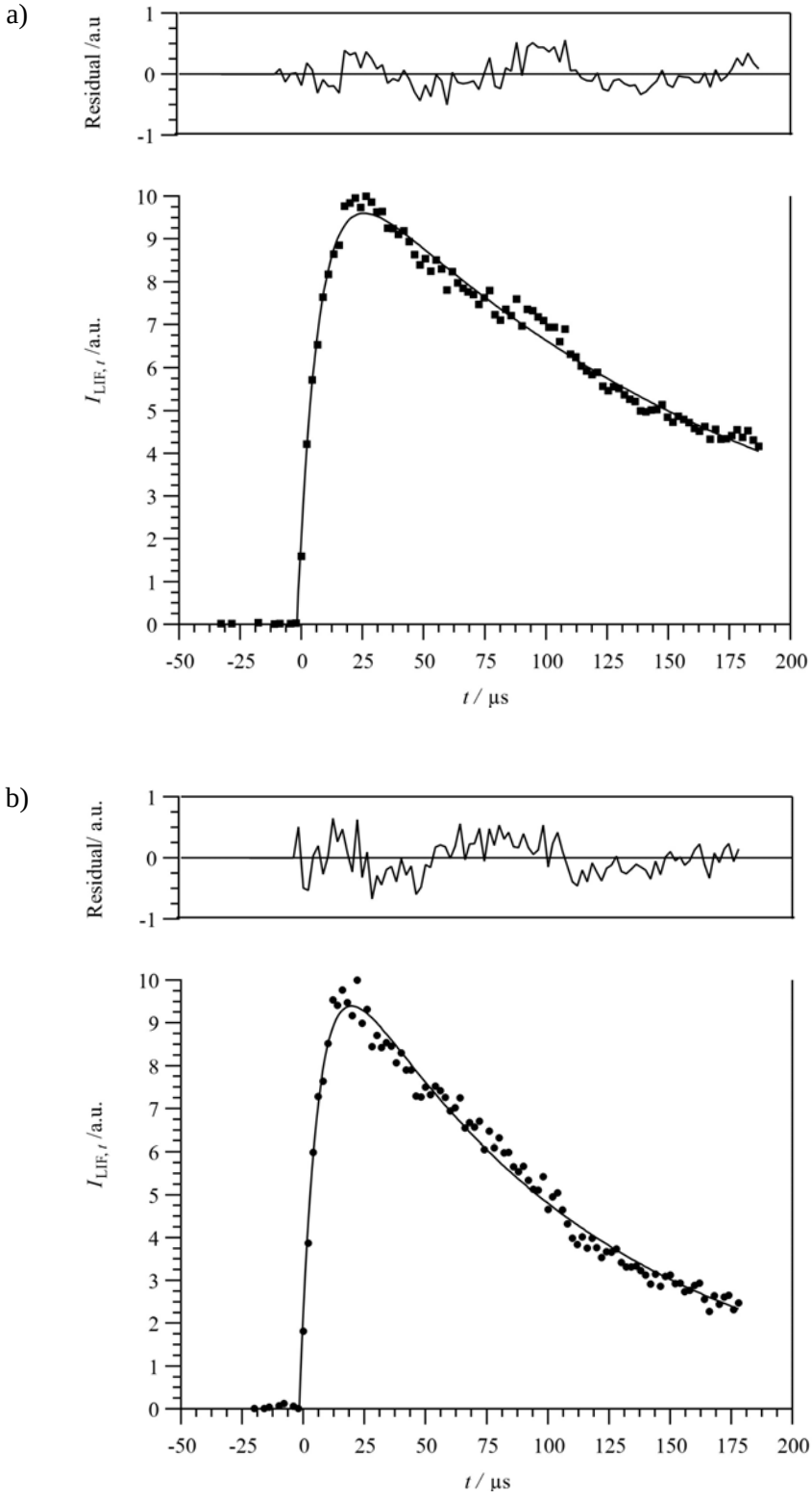

Figure 1. Temporal evolution of $I_{LIF,\,t}$ from OH radicals at 21.1 K in the presence of a) $[CH_3OH] = 3.43 \times 10^{13}$ molecule cm^{-3}. b) $[CH_3CH_2OH] = 4.10 \times 10^{13}$ molecule cm^{-3}. The residual shows the deviation of the data from the biexponential fit.

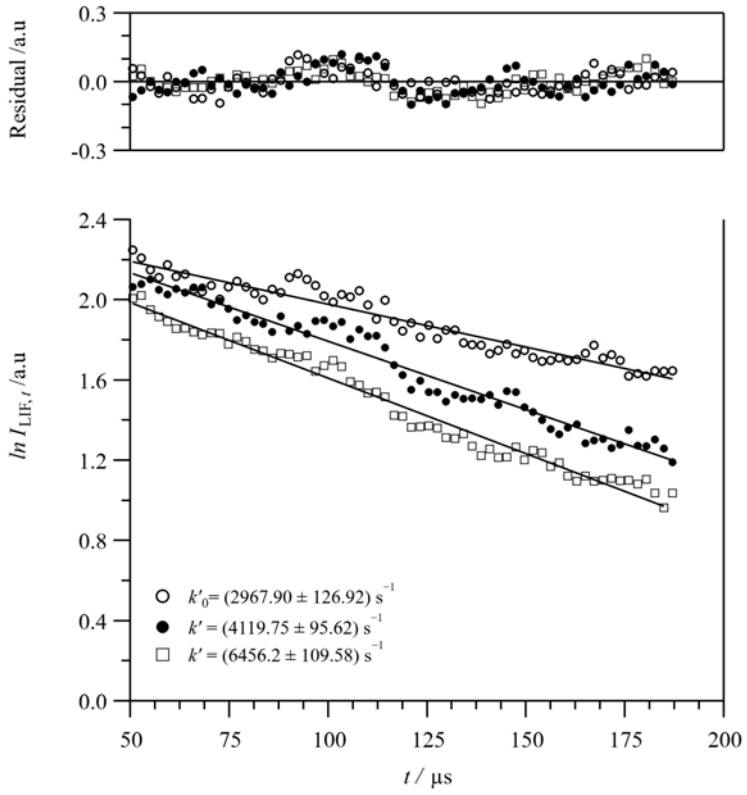

Figure 2. Plots of $ln\ I_{LIF,\,t}$ vs t. [CH_3OH] = 4.49 × 10^{13} (white squares), [CH_3OH] = 1.50 × 10^{13} (black circles) and in the absence of CH_3OH (black open circles), referred as k'_0, at 21.1 K and considering that the reaction time associated to the depletion of OH radical begins at t_0 = 50 μs. The upper panel, residual, shows the slight deviation of the values from the linear behaviour.

for ease of visualization; however more than 10 LIF experiments, and therefore k' values, were performed for subsequent analysis.

Finally, the temperature-dependent rate coefficient $k(T)$ is determined from the slope of k'-k'_0 versus [R] plots according to Eq. 7. More details about the analysis of the data can be found elsewhere [21].

$$k' - k'_0 = k(T)\,[R] \qquad \text{Eq. 7}$$

Figure 3 shows the change in the slope of the k'-k'_0 versus [H_2CO] that is clearly observed between 21.1 K and 107.0 K for the H_2CO + OH reaction, implying that the rate coefficient $k(T)$ increases from 107.0 K to 21.1 K.

RESULTS

Temperature dependence of $k(T)$

The results presented in this review have been deeply discussed in previous publications [7-9] and a PhD thesis [24]. In addition, a brief discussion concerning computational methods employed to calculate $k(T)$ at very low temperatures is also given.

In this section, the kinetic results for the reaction R1, R2, and R3 at very low temperatures are reviewed [7-13]. The final goal of the ultralow temperature kinetic studies is the inclusion of the temperature dependence of k(T) in kinetic databases to be finally used in astrochemical models. For a certain T-range, the temperature dependence of $k(T)$, commonly employed in the field of Astrochemistry, is given by Eq. 8 [25].

$$K(T) = \alpha\,(T/300K)^{\beta}\,\exp\,(-\gamma/T) \qquad \text{Eq. 8}$$

The experimental determination of α (in cm^3 $molecule^{-1}$ s^{-1}), β (unitless), and γ (in K) parameters are mandatory to obtain $k(T)$ at a given temperature within the investigated T-range. Extrapolation out of that T-range is risky as

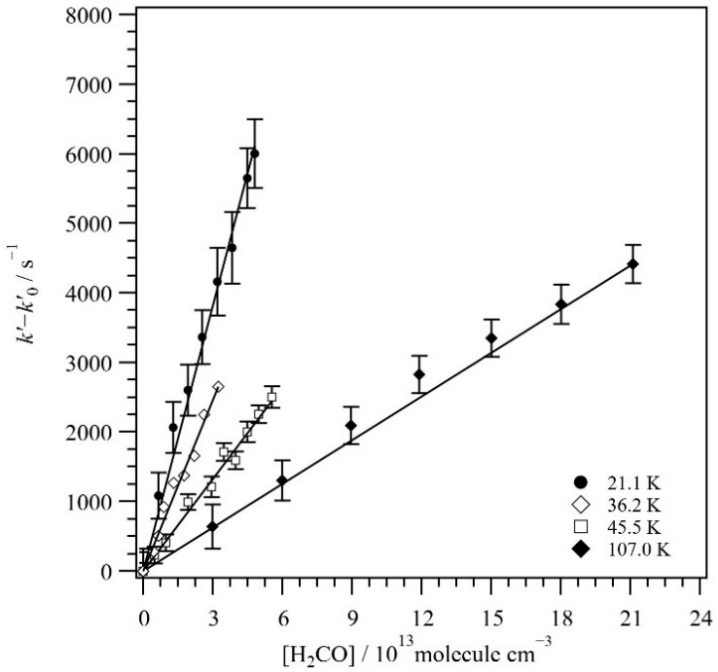

Figure 3. Examples of the k'-k'_0 versus [H_2CO] plots between 21.1 and 107 K.

$k(T)$ can be usually underestimated. The global rate coefficients, at temperatures operating in cold interstellar environments are summarized in Table 2 (between T = 11.7 K and T = 107.0 K). The results between 107.0 K and 202 K can be found in Table 3. It is important to mention that several experiments were made at the same T by changing the total pressure to study the potential pressure dependence which would make our data unsuitable to simulate the astrochemical networks. The results have shown that there is no pressure dependence taking into account the experimental uncertainties when gathering our results with previous data [7-13].

Kinetics of the H_2CO + OH reaction

For Reaction R1, the experimental kinetic data from Sivakumaran *et al*. [26] were the only available in the literature at temperatures below 298 K, until Ocaña *et al.* [7] recently published the temperature dependence of k(T) between 21.1 and 107 K. The data reported by Sivakumaran *et al.* [26] are consistent with the data reported by the UCLM research group at $T \leq 107$ K, as shown in Figure 4. The combination of both sets of experimental results let extend the T-dependence for $k(T)$ in the temperature range covered up to 300 K. The three-parameter expression valid in the 21.1-300 K range is:

$$k(21.1\text{–}300\text{K}) = (7.73 \pm 0.89) \times 10^{-12} (T/300\ \text{K})^{-(1.03\pm0.05)}\ \text{cm}^3\ \text{molecule}^{-1}\ \text{s}^{-1} \quad \text{Eq. 9}$$

where the errors are the standard deviation ±σ.

An enhancement of $k(T)$ at very low temperatures of more than one order of magnitude is observed with respect to that at room temperature. To physically interpret this enhancement of $k(T)$, many computational methods have been developed [7, 20, 27-29]. These methods can reproduce the experimental tendency, but only from a qualitative point of view. In this review, only the Quasi-classical Trajectory (QCT) calculations developed by the research group of Octavio Roncero (CSIC, Madrid) in collaboration with our research group are mentioned. These calculations are reinforced by a highly accurate potential energy surface (PES) developed for this purpose, and they reproduce the experimental behaviour [27], predicting that long-range dipole-dipole interactions can explain the formation of a pre-reaction complex OH-H_2CO sufficiently stable. The dynamical study of this system strongly predicts orthogonal vibrations that can

Table 2. Rate coefficients* for the reviewed OH-reactions between 11.7 and 107.0 K.

T_{typ}/K	T/K	n /10^{16} cm^{-3}	$k(T)$ H_2CO + OH	$k(T)$ CH_3OH + OH	$k(T)$ CH_3CH_2OH + OH	Reference
	11.7 ± 0.7	6.88 ± 0.62	-	9.38 ± 0.64	-	[9]
	13.0 ± 0.7	6.41 ± 0.55	-	7.77 ± 0.36	-	[9]
	14.3 ± 0.8	5.90 ± 0.52	-	8.78 ± 0.37	-	[9]
~21	22.1 ± 1.4	1.91 ± 0.25	-	5.57 ± 0.71	-	[9]
	21.1 ± 0.6	3.37 ± 0.15	10.1 ± 1.0	6.05 ± 0.22	13.1 ± 0.3	[7-9]
	22.5 ± 0.7	7.43 ± 0.32	12.0 ± 1.2	6.19 ± 0.17	12.3 ± 1.9	[7-9]
	21.7 ± 1.4	16.65 ± 1.61	12.3 ± 1.2	9.05 ± 0.41	12.9 ± 2.2	[7-9]
	22.4 ± 1.4	17.0 ± 1.6	-	4.30 ± 0.66	-	[10]
	36.2 ± 1.2	17.73 ± 0.86	8.6 ± 0.9	5.92 ± 0.29	10.9 ± 0.3	[7-9]
~45	45.5 ± 2.0	0.69 ± 0.08	4.4 ± 0.5	-	8.4 ± 0.8	[7, 8]
	47.7 ± 0.6	2.74 ± 0.09	-	2.17 ± 0.35	-	[9]
	45.3 ± 1.3	4.23 ± 0.28	-	4.08 ± 0.19	9.0 ± 0.6	[8, 9]
	42.5 ± 1.3	5.22 ± 0.33	-	2.74 ± 0.42	-	[10]
	42.6 ± 1.3	5.22 ± 0.33	-	-	9.3 ± 0.2	[8]
	45.6 ± 1.4	10.19 ± 0.52	6.1 ± 0.8	-	-	[7]
~50	50.5 ± 1.6	1.50 ± 0.12	-	2.70 ± 0.11	7.5 ± 0.2	[8, 9]
	51.6 ± 1.7	4.17 ± 0.35	4.2 ± 0.4	2.47 ± 0.15	7.2 ± 1.0	[7-9]
	51.6 ± 1.7	4.17 ± 0.35	-	2.19 ± 0.26	-	[10]
	52.2 ± 0.9	5.15 ± 0.13	-	2.97 ± 0.60	-	[10]
	49.9 ± 1.4	8.33 ± 0.41	-	3.30 ± 0.19	8.0 ± 0.3	[8, 9]
	52.1 ± 0.5	19.52 ± 0.28	-	2.93 ± 0.24	7.4 ± 0.8	[8, 9]
~55	55.4 ± 1.4	3.02 ± 0.23	4.1 ± 0.4	-	-	[7]
	56 ± 4	4.4 ± 0.5	-	4.9 ± 0.8	6.0 ± 0.5	[12, 13]
	54 ± 6	8 ± 1	-	-	5.5 ± 0.7	[13]
~63	61.0 ± 1.0	2.02 ± 0.08	-	2.11 ± 0.75	-	[10]
	64.1 ± 1.7	2.24 ± 0.15	-	-	6.7 ± 0.1	[8]
	64.2 ± 1.7	2.24 ± 0.15	-	1.47 ± 0.23	-	[10]
	63.0 ± 4.0	3 ± 1	-	4.2 ± 0.4	-	[11]
	64.1 ± 1.6	4.63 ± 0.27		2.91 ± 0.10	-	[9]
	64.4 ± 0.6	17.36 ± 0.29	-	-	6.7 ± 0.4	[8]

Table 2 continued..

T_{typ}/K	T/K	n /10^{16} cm^{-3}	$k(T)$ $H_2CO + OH$	$k(T)$ $CH_3OH + OH$	$k(T)$ $CH_3CH_2OH + OH$	Reference
~70	69.5 ± 1.6	3.26 ± 0.19	-	4.77 ± 0.21	4.2 ± 0.1	[8, 9]
	68.8 ± 0.6	16.58 ± 0.27	-	5.58 ± 0.32	4.5 ± 1.2	[8, 9]
~80	78.2 ± 1.0	2.45 ± 0.08	2.8 ± 0.3	-	3.0 ± 0.5	[7, 8]
	82.0 ± 4.0	5.1 ± 0.7	-	3.4 ± 0.5	-	[11]
	81.0 ± 4.0	8.9 ± 1.0	-	3.2 ± 0.5	-	[11]
	84 ± 4	12 ± 2	-	-	6 ± 2	[13]
	81.1 ± 0.5	14.49 ± 0.22	-	-	5.4 ± 0.4	[8]
	82 ± 3	16 ± 2	-	-	7 ± 3	[13]
	79.0 ± 4.0	17 ± 2	-	3.3 ± 0.6	-	[11]
~90	88 ± 5	3.5 ± 0.5	-	-	4.0 ± 0.6	[13]
	89 ± 3	6.5 ± 0.6	-	-	4.2 ± 0.2	[13]
	86 ± 3	6.8 ± 0.6	-	-	5 ± 2	[13]
	88 ± 8	9.4 ± 1.3	-	3.8 ± 0.4	-	[12]
	88 ± 4	11 ± 1	-	-	5.5 ± 0.6	[13]
	92.5 ± 0.5	13.09 ± 0.19	-	-	5.4 ± 0.4	[8]
	89.5 ± 0.6	18.24 ± 0.33	2.4 ± 0.3	4.83 ± 0.12	5.0 ± 1.4	[7-9]
	89.1 ± 0.7	43.38 ± 0.51	-	4.30 ± 0.22	-	[9]
~100	99.3 ± 0.4	7.67 ± 0.09	-	4.76 ± 0.05	4.3 ± 0.1	[8, 9]
	101.8 ± 0.6	18.34 ± 0.17	-	3.74 ± 0.08	-	[9]
~107	107.0 ± 0.5	4.90 ± 0.06	2.2 ± 0.2	2.03 ± 0.02	3.0 ± 0.2	[7-9]
	106.0 ± 0.6	14.02 ± 0.11	-	2.15 ± 0.07	-	[9]

*in 10^{-11} cm^3 molecule^{-1} s^{-1}. Stated uncertainties in $k(T)$ are the combination of the statistical and systematic (±10%) errors. Uncertainties are ±σ (standard deviation) for T and n.

exchange energy enough to pass through the barrier and consequently form the reaction products (HCO + H_2O). However, quantitatively, the calculated $k(T)$ is lower than the experimental ones. Such a discrepancy is due principally to two reasons: the collision probabilities depend directly on the PES, which is enough accurate to allow the reproduction of the experimental behaviour, but not for quantitative analysis and, more importantly, the quantum effects are neglected in this method. Consequently, and especially at very low temperatures, the redisocciation of the pre-reactive complex back to the reactants is overestimated and therefore, the rate coefficient is underestimated.

Kinetics of the CH_3OH + OH reaction

The gas-phase kinetics of reaction (R2) has been investigated by our research group, the Rennes group (France) and the Leeds group (UK) using

Table 3. Rate coefficients* for each molecule of interest in this work up to 202 K.

T_{typ}/K	T/K	$n/10^{16}$ cm^{-3}	$k(T)$ CH_3OH	$k(T)$ CH_3CH_2OH*	Reference
~123	115.3 ± 1.1	9.58 ± 0.14	1.85 ± 0.07	-	[9]
	123 ± 5[a]	3.15 ± 0.15	0.43 ± 0.21	-	[12]
	122.5 ± 1.0	7.20 ± 0.08	1.21 ± 0.04	-	[9]
~137	130 ± 5[a]	6.6 ± 0.3	0.39 ± 0.21	-	[12]
	133 ± 10	13 ± 3	-	3.6 ± 0.3	[13]
	138 ± 9	7.8 ± 1.0	0.53 ± 0.17	1.7 ± 0.2	[12, 13]
	136.1 ± 0.8	24.92 ± 0.35	1.83 ± 0.08	-	[9]
~143	140.4 ± 1.0	21.68 ± 0.40	1.24 ± 0.03	-	[9]
	143 ± 5[a]	2.76 ± 0.14	0.31 ± 0.12	-	[12]
	143.3 ± 0.6	17.02 ± 0.17	1.36 ± 0.03	-	[9]
	143 ± 15	18 ± 2	-	3.6 ± 0.8	[13]
~150	146 ± 15	26 ± 4	-	4 ± 1	[13]
	153.1 ± 0.7	9.14 ± 0.11	0.98 ± 0.04	-	[9]
	148 ± 15	10 ± 2	-	1.7 ± 0.4	[13]
	149.9 ± 0.7	10.69 ± 0.12	1.28 ± 0.10	-	[9]
	148.3 ± 0.6	12.35 ± 0.13	1.84 ± 0.04	-	[9]
~165	158.8 ± 0.6	7.40 ± 0.07	0.43 ± 0.02	-	[9]
	163 ± 5[a]	2.46 ± 0.13	0.17 ± 0.07	-	[12]
	165.7 ± 0.9	5.64 ± 0.08	0.17 ± 0.01	-	[9]
	177.5 ± 1.2	6.71 ± 0.11	0.071 ± 0.003	-	[9]
	180 ± 10[a]	1.59 ± 0.08	0.07 ± 0.02	-	[12]
	202 ± 2[a]	1.30 ± 0.06	0.060 ± 0.008	-	[12]

* in 10^{-11} cm^3 molecule^{-1} s^{-1}. [a] Flow tube technique. Stated uncertainties in $k(T)$ are the combination of the statistical and systematic (±10%) errors. Uncertainties are ±σ (standard deviation) for T and n.

the CRESU technique. The Leeds group also used a fast-flow reactor coupled to mass spectrometry to perform kinetic experiments up to 202 K. As can be seen in Figure 5, a total of four different studies on this reaction have been carried out below 220 K [9-12]. The rate coefficient was determined down to 11.7 K, temperature that can be found in dense molecular clouds of the ISM. The kinetic behaviour of this chemical system is a bit different from the H_2CO + OH reaction and we can define three different kinetic regimes. From 202 K up to 99.3 K there is a huge increment of

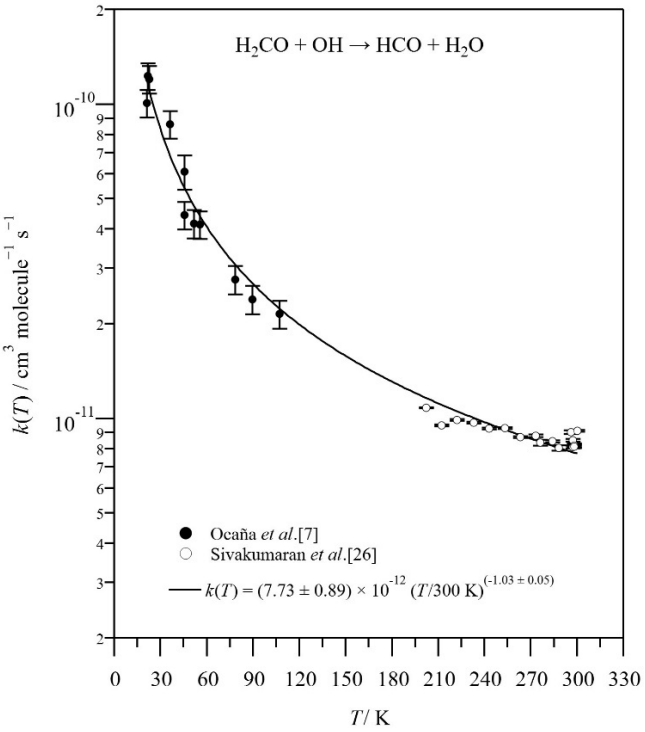

Figure 4. Temperature dependence of the rate coefficient for the OH + H_2CO reaction between 21.1 and 300 K.

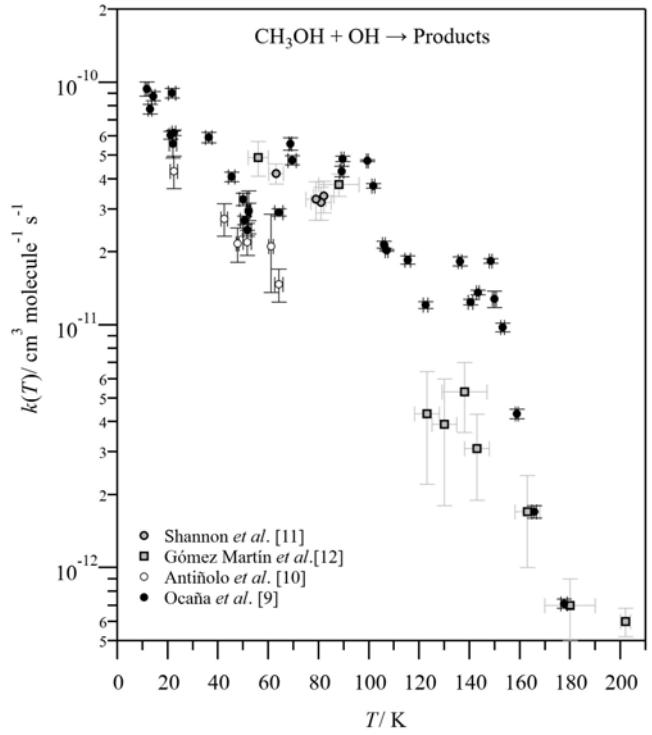

Figure 5. Temperature dependence of the rate coefficient for the CH_3OH + OH reaction down to 11.7 K reported by our research group and the Leeds group.

the rate coefficient $k(T)$; (k(202 K)/k(99.3 K) ~79 while from 99.3 K down to 22.5 K the increment of $k(T)$ is less pronounced (k(21.7 K)/k(99.3 K) ~2); for the last regime, in the temperature range from 22.5 K down to 11.7 K, $k(T)$ remains constant considering the experimental uncertainties. For that reason, a three-parameter expression for k(T) does not properly fit in the whole temperature range. For a narrow temperature range, Antiñolo *et al.* reported the following expression:

$$k(22–64\ \mathrm{K}) = (3.6 \pm 0.1) \times 10^{-12} (T/300\ \mathrm{K})^{-(1.0\pm0.2)}\ \mathrm{cm^3\ molecule^{-1}\ s^{-1}} \quad \text{Eq. 10}$$

In general, there is a reasonable agreement among all studies [10-12]. The slight discrepancies are mainly related to the experimental procedure and are associated with systematic errors; this is extensively discussed and justified in Ocaña *et al.* [9].

Due to the interest in this reaction in atmospheric chemistry as well as in combustion chemistry, the branching ratios for the formation of CH_3O radicals (product of reaction R2.1) and CH_2OH radicals (product of reaction R2.2) have been measured at room temperature and higher temperatures up to 1300 K, concluding that the CH_2OH radical is the major reaction product in that temperature range [30-32]. These findings were reinforced by theoretical studies which computed that the lower activation barrier of the CH_3OH + OH reaction corresponds to that forming CH_2OH [33-35]. From an experimental point of view, it is crucial to be able to detect the reaction products and to quantify the branching ratios as a function of temperature and more specifically at temperatures as close as possible to the lowest temperature found in molecular clouds (10 K). Laser-induced fluorescence technique is usually not appropriate for this kind of investigations, because it does not deliver an absolute value of the product density and not all products present a LIF spectrum. The combination of the chirped pulsed microwave spectroscopy and CRESU techniques developed in A. Suits' group is a promising technique that allows the detection and quantification of polar molecules by microwave absorption [36]. In addition, the Rennes group (France) have recently tuned a new experimental set-up, coupling this technique to a CRESU apparatus [37, 38]. Besides, mass spectrometry techniques are also of great interest provided that a tunable frequency source is used to photoionize the products without fragmentation. In the Rennes group, a CRESU apparatus has recently been built and implemented at the SOLEIL synchrotron to achieve this challenging task [39].

At very low temperatures, where the quantum effects are relevant, the measurement of branching ratios, taking advantage of the isotopic kinetic effect, have not experimentally been performed yet. Nevertheless, using laser-induced fluorescence spectroscopy, the Leeds group experimentally confirmed that CH_3O was formed in reaction R2.1 at 82 K [11]. These authors also evidenced from theoretical calculations that the reaction channel leading to CH_3O instead of CH_2OH becomes relevant at low temperatures [11]. This reaction seems to proceed through the formation of a pre-reactive complex, evolving to the products through the barrier controlled by the imaginary frequency of the transition state, and the computations concur in the highest imaginary frequency of the transition state corresponding to the channel leading to the formation of CH_3O [9, 35, 40, 41]. This seems to be a contradiction; however, the energy barrier leading to CH_3O radical is thinner than the one forming CH_2OH, which facilitates the QMT through the barrier to form the CH_3O radical [20, 28, 40]. From a computational point of view, there are some disagreements with regard to the importance of the reaction channel forming CH_3O at low temperatures depending on the methodology and assumptions inherent to these procedures. In this review, only some remarks are provided concerning the computational method developed by Luc Vereecken (Forschungszentrum Jülich, Germany) [9]. The methodology is based on a transition state theory (TST) formalism known as Multi Conformer Canonical Transition State Theory (MC-TST). The calculations presume that at the lowest temperature (T~10 K) the global rate coefficient becomes practically independent with pressure and that both products are equally important at interstellar conditions. More information about the computational methods can be found in reference [9].

Kinetics of the CH_3CH_2OH + OH reaction

For the CH_3CH_2OH + OH reaction, there are two kinetic studies at ultralow temperatures. In Figure 6 the results published by Ocaña *et al*. [8] (21.1-107.0 K, first study at T<54 K), and by Caravan *et al*. [13] (54-148 K) are presented.

Ocaña *et al.* [8] reported the following three-parameter expression in the investigated temperature range:

$$k(21.1\text{-}107.0\ \text{K}) = (2.10 \pm 0.25) \times 10^{-11} (T/300\ \text{K})^{-(0.71\pm0.05)}\ \text{cm}^3\ \text{molecule}^{-1}\ \text{s}^{-1} \quad \text{Eq. 11}$$

where the uncertainties are the standard deviation ±σ.

As stated all over this review, knowing the product branching ratios for reaction (R3) is crucial to provide useful data for astrochemical modellers. Experimentally, this information is only available at temperatures between 298 and 523 K from measured kinetic isotopic effects by Carr *et al.* [19]. According to this work, the channel corresponding to the formation of ethoxy (CH_3CH_2O) radical is negligible compared with the other two channels, *i.e.* the abstraction of the α-hydrogen forming CH_3CHOH (branching ratio of 0.75-0.9) and the abstraction of the β-hydrogen forming CH_2CH_2OH (branching ratio of 0.25-0.1). From a theoretical point of view, only a few studies focused at temperatures higher than 200 K predicted that the main channel is the one forming CH_3CHOH [35, 42-44]. On the other hand, and considering the previous success of the Leeds group detecting the CH_3O radical as the main product of the reaction of CH_3OH + OH by LIF [11], they attempted to detect the CH_3CH_2O radical using the same methodology but failed [13]. However, the hydrogen abstraction proceeds through the formation of a long-lived pre-reactive complex which evolves to the products, as stated in the introduction and for reaction 2. This reaction path to the products is controlled by the

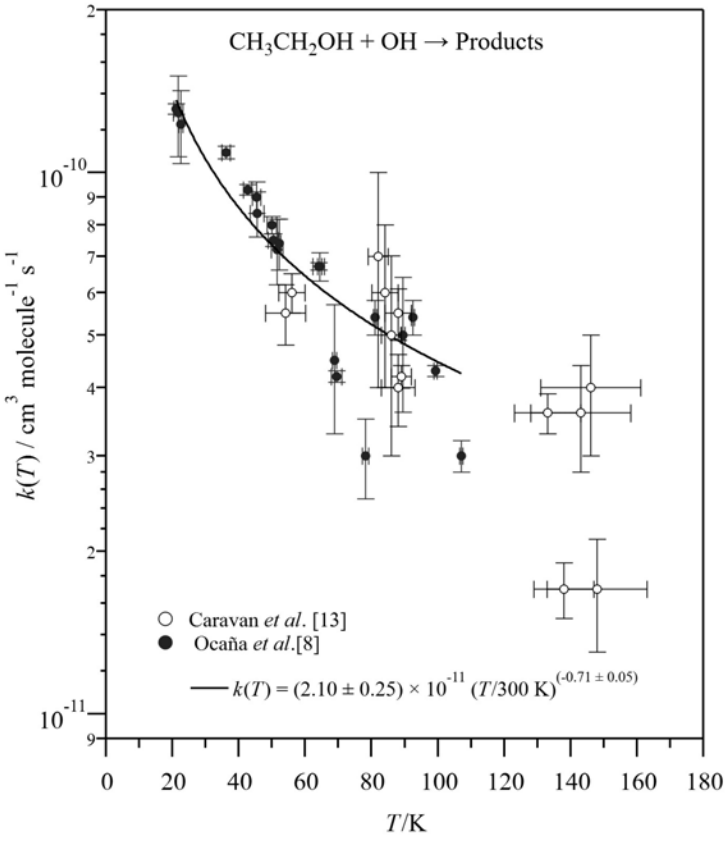

Figure 6. Temperature dependence of the rate coefficient of the OH + CH_3CH_2OH reaction between 21.1 and 148 K.

oscillatory imaginary frequency of the transition state, which is inversely related to the barrier width [6, 45, 46]. The computed imaginary frequency of the transition state that yields CH_3CH_2O is higher than that for the other two transition states [35, 42-44]. That is, at low temperatures, the ethoxy radical is expected to be the main product contrary to what was reported at high temperatures. Nevertheless, this is not conclusive and to unravel the reaction branching ratios of this reaction at very low temperatures, more computational and experimental studies are needed.

ASTROPHYSICAL IMPLICATIONS & CONCLUSIONS

The Kinetic Database for Astrochemistry (KIDA) and the University of Manchester Institute of Science and Technology (UMIST) database for Astrochemistry are the most relevant kinetic datasets undertaking their free code based on astrochemical networks [25, 47]. Despite the discovery of the enhancement of the rate coefficient for OH-molecule reactions at very low temperatures, due to the lack of experimental data, the rate coefficient for most of the neutral-neutral reactions is obtained from the extrapolation of high-temperature kinetic data. The results reviewed in this manuscript have been already included in the KIDA database to make them easily available for the scientific community. Furthermore, the experimental results obtained by the UCLM group have been already employed in complex astrochemical models, like the one developed by J. Cernicharo's group (CSIC-Madrid) to model the abundance of HCO and CH_3O radicals detected by astronomers in dark molecular clouds [7, 10].

The impact of this work on interstellar chemistry can be stressed when applying the experimental $k(T)$ values to previous works that consider an arbitrary value for the rate coefficient as the model developed for prestellar cores chemistry by Bacmann and Faure [15]. This model ends up predicting an abundance of the HCO and CH_3O radicals proportional to the rate coefficient of R1 (k_1) and R2.1 ($k_{2.1}$) as follows.

$$[HCO]/[H_2CO] = 8 \times k_1/k_4 \quad \text{Eq. 12}$$

$$[CH_3O]/[CH_3OH] = 8 \times k_{2.1}/k_5 \quad \text{Eq. 13}$$

where k_4 and k_5 are the rate coefficients for the reaction of a cation HX^+ with HCO and CH_3O, respectively.

$$HCO + HX^+ \rightarrow HCOX + X \quad \text{(R4)}$$

$$CH_3O + HX^+ \rightarrow CH_3OH^+ + X \quad \text{(R5)}$$

HX: any combination to form a positive ion that can easily give a proton (e.g. H_3^+).

For HCO, Bacmann and Faure employed a recommended value of 10^{-11} cm^3 s^{-1} for R1 and a typical value for the capture rate coefficient of 5×10^{-8} cm^3 s^{-1} for R4 (same for R5). Considering the rate coefficient k_1 of 10^{-11} cm^3 s^{-1}, this model underestimates the relative abundance of HCO with respect to H_2CO in prestellar cores. A value of 4×10^{-10} cm^3 s^{-1} would be needed to reproduce the observed abundances, [HCO] ~0.05 [H_2CO]. Taking into account the reviewed experimental results, the extrapolated $k(T)$ at 10 K using Eq. 9 results in k(10 K) ~2.6×10^{-10} cm^3 s^{-1} which is still lower, but closer to the value to reproduce the observed [HCO]/[H_2CO] ratio.

As mentioned in the introduction, the CH_3OH + OH reaction can proceed through two hydrogen abstraction channels forming water and CH_3O or CH_2OH radicals. In the Bacmann and Faure's model, [CH_3O]/[CH_3OH] ratio was simulated using a branching ratio of 100% for R2.1 and $k_{2.1}$ = 5×10^{-11} cm^3 s^{-1}, based on the results reported at ~50 K by the Leeds research group [12]. The obtained [CH_3O]/[CH_3OH] ~0.007 is slightly lower than that measured observationally, [CH_3O] ~0.01 [CH_3OH]. Taking advantage of the reviewed results down to 11.7 K published by the UCLM research group [9], k(11.7 K) = $(9.38 \pm 0.64) \times 10^{-11}$ cm^3 s^{-1}, and using a branching ratio of 1 for R2.1 channel, a value for [CH_3O]/[CH_3OH] ratio of [CH_3O] ~0.015 [CH_3OH] is found, which is much closer to observed values. However, this is considering CH_3O as the sole reaction product, which is questioned by the most recent computational study [9]. In any case, even if the branching ratio of this reaction is 50% for each product, this model reproduces reasonably well the observations in prestellar cores.

To model the abundance of HCO in other astrochemical environments, such as dark molecular clouds, a model has been run to simulate the evolution of the relative abundances to H-nuclei over a timescale of 10^7 years by using the two chemical networks mentioned above, UMIST and KIDA [7]. Despite R1 is fast at ultra-low temperatures, the results from the model reveal that it is not the main channel to form HCO in dark molecular clouds and the major route leading to the formation of HCO is the reaction between CH_2 radicals and O atoms (R6) [48]. UMIST propose to use a *T*-independent value of $k_6 = k(10 – 300\ \text{K}) = 5 \times 10^{-11}\ \text{cm}^3\ \text{s}^{-1}$, while KIDA recommends a smaller value $k_6 = k(10 - 300\ \text{K}) = 2 \times 10^{-12}\ \text{cm}^3\ \text{s}^{-1}$ [25, 47]. This uncertaintiy evidences the lack of accurate rate coefficients for use in astrochemical models. Further studies are needed to clarify the impact of the rate coefficient reported at very low temperatures for R1 to evaluate its implications in the chemistry of other environments such as diffuse clouds and photon-dominated regions (PDRs).

In 2012 the CH_3O radical was observed, for the first time, in a dark molecular cloud (Barnard 1b, hereafter B1-b), where the gas kinetic temperature was determined in the range of 10-15 K [17]. Taking into consideration the observed abundance of CH_3OH in B1-b [49], the $[CH_3O]/[CH_3OH]$ ratio reported was $\sim 3 \cdot 10^{-3}$ [17]. On the other hand, the CH_2OH radical has not been detected in any astrochemical source, yet. The rate coefficient for reaction R2 reported at 11.7 K can help to explain the observed abundances in this astrochemical environment by including it in the chemical models. The abundances of CH_3O, CH_3OH and OH involved in the CH_3OH + OH reaction have been previously modelled using both pure gas-phase models and gas-grain models that also consider the formation of CH_3O onto grain surfaces [5, 10, 50, 51] and a complex multivariant gas-grain network [52]. An extrapolated k(10 K) for the gas-phase CH_3OH + OH reaction from available *T*-expressions was employed in these models. Using a pure gas-phase model, Antiñolo *et al.* [10] calculated a value by extrapolation from the modified Arrhenius equation of $k(10\ \text{K}) = 1.1 \times 10^{-10}\ \text{cm}^3\ \text{s}^{-1}$ reported in CRESU measurements between 22 and 64 K (Eq. 10) over a total timescale of 10^5-10^7 years. The value of k(10 K) employed has been validated by Ocaña *et al.* [9], where $k(11.7\ \text{K}) = (9.38 \pm 0.64) \times 10^{-10}\ \text{cm}^3\ \text{s}^{-1}$. However, despite this model can reproduce the observed abundances for an evolving time of 10^7 years, it needs to be considered that the most recent computational study questioned that CH_3O is the sole reaction product [9].

Finally, the CH_3CH_2OH + OH reaction was not included in astrochemical kinetic databases due to the pressure dependence observed by the Leeds group. Note that a pressure-dependent reaction is expected to be very slow at extremely low pressures of the ISM. Nevertheless, the UCLM group did not observe a pressure dependence of $k_3(T)$, changing the previous assumptions, and their results are already included in the KIDA database [8]. Additional investigations would be certainly worthwhile to disentangle this situation. For instance, even lower gas densities should be explored to see whether the rate coefficient remains unaltered or not. From an astrochemical point of view, this reaction was recently considered as the starting point for the formation of other organic molecules such as formic acid, acetic acid, acetaldehyde, formaldehyde and glycolaldehyde in interstellar environments, concretely, in hot corinos ($T \sim 100$ K) [18]. However, none of the possible radical products of reactions 3.1-3.3 has been detected, until now, in the ISM despite the efforts of the astronomers.

The importance of this kind of investigations has been illustrated in this review to expand our knowledge of our cosmic past and future, concluding that further efforts are needed in this field. It is necessary to bring the stars to the laboratory.

ACKNOWLEDGMENTS

The results presented in this work, as well as the human resources involved, were partially supported by the European Research Council (NANOCOSMOS, SyG-610256), the Spanish Ministerio de Ciencia e Innovación (ASTROMOL, CSD2009-00038) and the Spanish Ministerio de Economía y Competitividad (MINECO) projects (GASSOL, CGL2013-43227-R). A. J. Ocaña would like to thank UCLM for funding (Plan Propio de Investigación).

CONFLICT OF INTEREST STATEMENT

There are no conflicts of interest to declare.

ABBREVIATIONS

BRs	:	Branching Ratios
COMs	:	Complex Organic Molecules
CRESU	:	French acronym of *Cinétique de Réaction en Ecoulement Supersonique Uniforme*.
ISM	:	Interstellar Medium
LIF	:	Laser-Induced Fluorescence
PDRs	:	Photon Dominated Regions
PES	:	Potential Energy Surface
PLP	:	Pulsed Laser Photolysis
QCT	:	Quasi-Classical Trajectory
QMT	:	Quantum Mechanical Tunneling

REFERENCES

1. McGuire, B. A. 2018, Astrophys. J. Suppl. Ser., 239, 17.
2. Millar, T. J. 2015, Astrochem. Plasma Sour. Sci. Technol., 24, 043001.
3. Bertin, M., Romanzin, C., Doronin, M., Philippe, L., Jeseck, P., Ligterink, N., Linnartz, H., Michaut, X. and Fillion, J.-H. 2016, Astrophys. J., 817, L12.
4. Féraud, G., Bertin, M., Romanzin, C., Dupuy, R., Le Petit, F., Roueff, E., Philippe, L., Michaut, X., Jeseck, P. and Fillion, J.-H. 2019, ACS Earth Sp. Chem., 3, 1135-1150.
5. Balucani, N., Ceccarelli, C. and Taquet, V. 2015, Mon. Not. R. Astron. Soc. Lett., 449, L16-L20.
6. Heard, D. E. 2018, Acc. Chem. Res., 51, 2620-2627.
7. Ocaña, A. J., Jiménez, E., Ballesteros, B., Canosa, A., Antiñolo, M., Albaladejo, J., Agúndez, M., Cernicharo, J., Zanchet, A., del Mazo, P., Roncero, O. and Aguado, A. 2017, Astrophys. J., 850, 28.
8. Ocaña, A. J., Blázquez, S., Ballesteros, B., Canosa, A., Antiñolo, M., Albaladejo, J. and Jiménez, E. 2018, Phys. Chem. Chem. Phys., 20, 5865-5873.
9. Ocaña, A. J., Blázquez, S., Potapov, A., Ballesteros, B., Canosa, A., Antiñolo, M., Vereecken, L., Albaladejo, J. and Jiménez, E. 2019, Phys. Chem. Chem. Phys., 21, 6942-6957.
10. Antiñolo, M., Agúndez, M., Jiménez, E., Ballesteros, B., Canosa, A., Dib, G. El, Albaladejo, J. and Cernicharo, J. 2016, Astrophys. J., 823, 25.
11. Shannon, R. J., Blitz, M. A., Goddard, A. and Heard, D. E. 2013, Nat. Chem., 5, 745-749.
12. Gómez Martín, J. C., Caravan, R. L., Blitz, M. A., Heard, D. E. and Plane, J. M. C. 2014, J. Phys. Chem. A., 118, 2693-2701.
13. Caravan, R. L., Shannon, R. J., Lewis, T., Blitz, M. A. and Heard, D. E. 2015, J. Phys. Chem. A., 119, 7130-7137.
14. Atkinson, R., Baulch, D. L., Cox, R. A., Crowley, J. N., Hampson, R. F., Hynes, R. G., Jenkin, M. E., Rossi, M. J. and Troe, J. 2006, Atmos. Chem. Phys., 6, 3625-4055.
15. Bacmann, A. and Faure, A. 2016, Astron. Astrophys., 587, A130.
16. Liszt, H. S., Pety, J. and Lucas, R. 2008, Astron. Astrophys., 486, 493-496.
17. Cernicharo, J., Marcelino, N., Roueff, E., Gerin, M., Jiménez-Escobar, A. and Muñoz Caro, G. M. 2012, Astrophys. J. Lett., 759, 2010-2013.
18. Skouteris, D., Balucani, N., Ceccarelli, C., Vazart, F., Puzzarini, C., Barone, V., Codella, C. and Lefloch, B. 2018, Astrophys. J., 854, 135.
19. Carr, S. A., Blitz, M. A. and Seakins, P. W. 2011, J. Phys. Chem. A., 115, 3335-3345.
20. Naumkin, F., del Mazo-Sevillano, P., Aguado, A., Suleimanov, Y. V. and Roncero, O. 2019, ACS Earth Sp. Chem., 3, 1158-1169.
21. Jiménez, E., Ballesteros, B., Canosa, A., Townsend, T. M., Maigler, F. J., Napal, V., Rowe, B. R. and Albaladejo, J. 2015, Rev. Sci. Instrum., 86, 45108.
22. Taylor, S. E., Goddard, A., Blitz, M. A., Cleary, P. A. and Heard, D. E. 2008, Phys. Chem. Chem. Phys., 10, 422-437.
23. Canosa, A., Ocaña, A. J., Antiñolo, M., Ballesteros, B., Jiménez, E. and Albaladejo, J. 2016, Exp. Fluids., 57, 1-14.
24. Ocaña, A. J. 2020, Gas-phase reactivity of the OH radical with oxygenated organic molecules at interstellar conditions (T = 21−107 K) by using a new pulsed CRESU technique., University of Castilla-La Mancha.

25. Wakelam, V., Loison, J. C., Herbst, E., Pavone, B., Bergeat, A., Béroff, K., Chabot, M., Faure, A., Galli, D., Geppert, W. D., Gerlich, D., Gratier, P., Harada, N., Hickson, K. M., Honvault, P., Klippenstein, S. J., Picard, S. D. L., Nyman, G., Ruaud, M., Schlemmer, S., Sims, I. R., Talbi, D., Tennyson, J. and Wester, R. 2015, Astrophys. Journal, Suppl. Ser., 217, 20.
26. Sivakumaran, V., Hölscher, D., Dillon, T. J. and Crowley, J. N. 2003, Phys. Chem. Chem. Phys., 5, 4821-4827.
27. Zanchet, A., del Mazo, P., Aguado, A., Roncero, O., Jiménez, E., Canosa, A., Agúndez, M. and Cernicharo, J. 2018, Phys. Chem. Chem. Phys., 20, 5415-5426.
28. del Mazo-Sevillano, P., Aguado, A., Jiménez, E., Suleimanov, Y. V. and Roncero, O. 2019, J. Phys. Chem. Lett., 10, 1900-1907.
29. del Mazo-Sevillano, P., Aguado, A. and Roncero, O. 2021, J. Chem. Phys., 154, 094305.
30. McCaulley, J. A., Kelly, N., Golde, M. F., and Kaufman, F. 1989, J. Phys. Chem., 93, 1014-1018.
31. Matsumi, Y., Inagaki, Y. and Kawasaki, M. 1994, J. Phys. Chem., 98, 3777-3781.
32. Liu, D., Giri, B. R. and Farooq, A. 2019, Proc. Combust. Inst., 37, 153-162.
33. Pardo, L., Banfelder, J. R. and Osman, R. 1992, J. Am. Chem. Soc., 114, 2382-2390.
34. Jodkowski, J. T., Rayez, M.-T., Rayez, J.-C., Bérces, T. and Dóbé, S. 1999, J. Phys. Chem. A., 103, 3750-3765.
35. Xu, S. and Lin, M. C. 2007, Proc. Combust. Inst., 31, 159-166.
36. Abeysekera, C., Zack, L. N., Park, G. B., Joalland, B., Oldham, J. M., Prozument, K., Ariyasingha, N. M., Sims, I. R., Field, R. W. and Suits, A. G. 2014, J. Chem. Phys., 141, 214203.
37. Guillaume, T., Gupta, D., Hays, B., Cooke, I., Abdelkader Khedaoui, O., Hearne, T. and Sims, I. 2021, Bull. Am. Phys. Soc., X26.00003.
38. Hays, B. M., Guillaume, T., Hearne, T. S., Cooke, I. R., Gupta, D., Abdelkader Khedaoui, O., Le Picard, S. D. and Sims, I. R. 2020, J. Quant. Spectrosc. Radiat. Transf., 250, 107001.
39. Bourgalais, J., Caster, K. L., Durif, O., Osborn, D. L., Le Picard, S. D. and Goulay, F. 2019, J. Phys. Chem. A., 123, 2178-2193.
40. Gao, L. G., Zheng, J., Fernández-Ramos, A., Truhlar, D. G. and Xu, X. 2018, J. Am. Chem. Soc., 140, 2906-2918.
41. Roncero, O., Zanchet, A. and Aguado, A. 2018, Phys. Chem. Chem. Phys., 20, 25951-25958.
42. Galano, A., Alvarez-Idaboy, J. R., Bravo-Pérez, G. and Ruiz-Santoyo, M. E. 2002, Chem. Chem. Phys., 4, 4648-4662.
43. Sivaramakrishnan, R., Su, M.-C., Michael, J. V., Klippenstein, S. J., Harding, L. B. and Ruscic, B. 2010, J. Phys. Chem. A., 114, 9425-9439.
44. Zheng, J. and Truhlar, D. G., 2012, Faraday Discuss., 157, 59-88.
45. Schwartz, M., Marshall, P., Berry, R. J., Ehlers, C. J. and Petersson, G. A. 1998, J. Phys. Chem. A., 102, 10074-10081.
46. Bell, R. P. 1980, The tunnel effect in chemistry, Springer, Boston.
47. McElroy, D., Walsh, C., Markwick, A. J., Cordiner, M. A., Smith, K. and Millar, T. J. 2013, Astron. Astrophys., 550, A36.
48. Agúndez, M., Cernicharo, J. and Guélin, M. 2015, Astron. Astrophys., 577, L5.
49. Öberg, K. I., Bottinelli, S., Jorgensen, J. K., and van Dishoeck, E. F. 2010, Astrophys. J., 716, 825-834.
50. Vasyunin, A. I. and Herbst, E. 2013, Astrophys. J., 769, 34.
51. Ruaud, M., Loison, J. C., Hickson, K. M., Gratier, P., Hersant, F. and Wakelam, V. 2015, Mon. Not. R. Astron. Soc., 447, 4004-4017.
52. Acharyya, K., Herbst, E., Caravan, R. L. L., Shannon, R. J. J., Blitz, M. A. A. and Heard, D. E. 2015, Mol. Phys., 113, 2243-2254.